GDCh Research Article Angewandte International Edition Chemie www.angewandte.org

Check for updates

How to cite: *Angew. Chem. Int. Ed.* **2025**, *64*, e202511775
doi.org/10.1002/anie.202511775

MOFs Hot Paper

Decoration of Metal-Organic Frameworks with Coenzyme Mimics for Boosting Photocatalytic Hydrogen Production

*Yongjie Li, Jiajia Huang, Ming-Liang Gao, Xiyuan Zhang, Siyu Chen, Jing-Yao Liu, and Hai-Long Jiang**

Abstract: Despite remarkable progress achieved in biomimetic catalysis, the majority of studies have primarily concentrated on mimicking the structures of catalytic sites in metalloenzymes, while frequently neglecting the crucial roles of multifunctional coenzymes therein. In this study, the coenzyme mimics of nicotinic acid (NA) and 3-carboxy-1-methylpyridinium iodide (NA-Me, simply denoted as NM) have been modified onto the metal-organic framework UiO-66-NH_2, affording UiO-66-X (X=NA, NM) with varying the degree of mimicry for the nicotinamide nucleotide coenzyme. Remarkably, UiO-66-NM showcases approximately five- and seven-fold activity higher than UiO-66-NA and the pristine UiO-66-NH_2, respectively, in the photocatalytic hydrogen production. Both experimental and computational results reveal that the NM dangling on the MOF undergoes structural redox change similar to that in the regeneration process of NAD(P)H coenzyme, which serves as the proton and electron relays surrounding catalytic Pt sites, facilitating proton-coupled electron transfer (PCET) and thereby boosting photocatalytic activity. This work offers new insights and strategies for the design and fabrication of biomimetic heterogeneous catalysts.

Introduction

Enzymes promote reactions at high rates and enable selective formation of products under mild conditions.[1] As crucial motifs of natural enzymes, coenzymes can directly participate in redox reactions and indirectly influence enzyme conformation and intermediate binding via microenvironment modulation, accordingly playing vital roles in regulating enzyme activity and selectivity.[2] However, the use of natural enzymes in industrial processes is limited to their instability outside the living environment and the high costs of isolation and purification.[3] Therefore, it is necessary to develop artificial enzyme systems that mimic the enzymatic mechanism but can operate under practical conditions.[4,5]

Owing to the distinctive advantages of natural enzymes as efficient catalysts, biomimetic catalysis has emerged as a crucial and foundational branch in catalytic field since the 1970s.[6,7] The biomimetic studies have long focused on mimicking the structures of catalytic sites within enzymes.[8,9] In recent years, the development of artificial enzymes has gradually shifted its attention to the cofactors surrounding the catalytic centers.[10–12] The cofactors, generally including prosthetic group and coenzyme, are necessary to guarantee the exceptional catalytic performance of enzymes. Unfortunately, the strict operation conditions, such as pH and temperature, required for natural coenzymes, along with the complexity of their regeneration mechanisms, hinder the effective integration into biomimetic catalytic systems.[13,14] The creation of artificial coenzymes is of great significance, as it ensures a working mechanism analogous to that of natural systems, thereby maintaining their efficiency.[15,16] Accordingly, suitable biomimetic materials possessing well-defined enzyme-like pockets and precise structural tailorability, and ensuring stability are required to create artificial coenzymes and achieve biomimetic catalysis.[17–19]

As a class of crystalline porous materials, metal-organic frameworks (MOFs) featuring high porosity, well-defined and tailorable structures, would be an ideal platform for constructing biomimetic catalytic systems.[20–22] Particularly, the customizable pores in MOFs can serve as the biomimetic catalytic pockets constructing dynamic interactions with coenzyme molecules.[11,23,24] The structural tailorability of MOFs enables accurate modulation of chemical microenvironment around catalytic sites for improved catalytic performance.[25–27] Meanwhile, MOF-based (co)enzyme-mimicking catalysts with precise structures would be of significance toward understanding the biomimetic catalytic mechanisms.[15,28] Unfortunately, to our knowledge, though biomimetic catalysis has been intensively investigated with MOFs,[22,28] coenzyme-mimicking microenvironment modulation around catalytic sites based on MOFs has not yet been reported thus far.

In this work, the biomimetic catalyst UiO-66-NM has been synthesized by grafting 3-carboxy-1-methylpyridinium

[*] Y. Li, Dr. J. Huang, Dr. M.-L. Gao, X. Zhang, S. Chen, Prof. Dr. H.-L. Jiang
Hefei National Research Center for Physical Sciences at the Microscale, Department of Chemistry, School of Chemistry and Materials Science, University of Science and Technology of China, Hefei, Anhui 230026, P.R. China
E-mail: jianglab@ustc.edu.cn

Prof. Dr. J.-Y. Liu
Laboratory of Theoretical and Computational Chemistry, Institute of Theoretical Chemistry, College of Chemistry, Jilin University, Changchun, Jilin 130023, P.R. China

Additional supporting information can be found online in the Supporting Information section

© 2025 Wiley-VCH GmbH

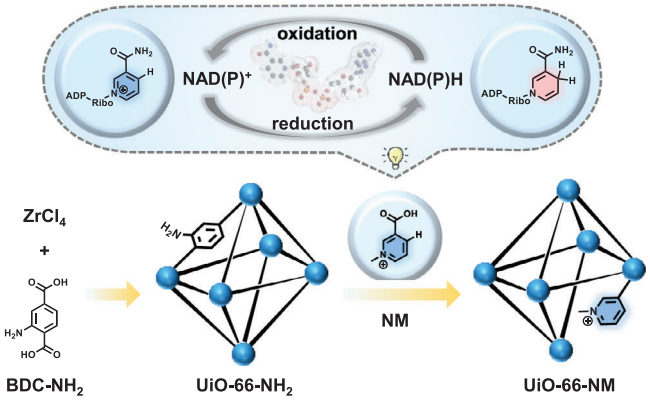

Scheme 1. Schematic illustration showing biomimetic design and rational fabrication of UiO-66-NM, involving NM as a redox-active coenzyme mimetics, inspired by the coenzyme regeneration mechanism of NAD(P)H.

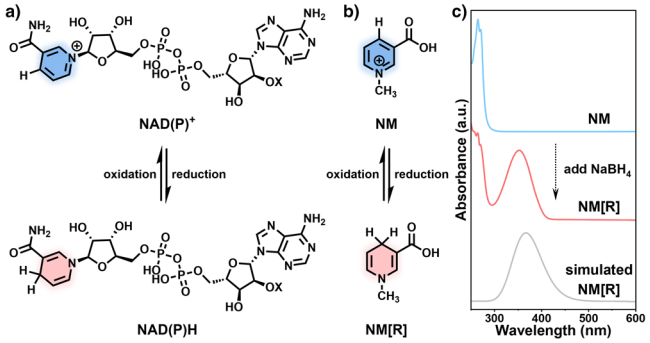

Figure 1. a) The redox tautomeric structures of NAD(P)$^+$/NAD(P)H (NAD$^+$: X = -H; NADP$^+$: X = -PO_3^{2-}). b) The supposed corresponding redox tautomeric structures of NM molecules. c) UV–vis spectra of NM before and after adding $NaBH_4$ and compared with theoretical simulation of NM[R].

iodide (NA-Me, simply denoted as NM) molecules onto photo-responsive UiO-66-NH_2 by post-synthetic modification, affording a structure/function dual-bionic system for NAD(P)H coenzyme (Scheme 1). Remarkably, the photo-mediated redox of NM molecules dangled on the MOF is found to significantly promote photocatalytic performance. As a result, UiO-66-NM exhibits excellent activity toward photocatalytic hydrogen production rate of 381 μmol g^{-1} h^{-1} under visible light irradiation, approximately 7 times that of the pristine UiO-66-NH_2, in the presence of Pt NPs as cocatalyst. Combined theoretical and experimental results confirm the NM-involved coenzyme-regeneration-mimicking mechanism. This mechanism enhances the separation of photogenerated electrons and holes, effectively lowering the energy barrier of the reaction and boosting the activity. This study, for the first time, demonstrates the mimicking of coenzyme structure and function based on MOFs for enhanced performance in heterogeneous photocatalytic systems.

Results and Discussion

Nicotinamide nucleotide coenzymes exist in two primary forms: reduced nicotinamide adenine dinucleotide (NADH) and reduced nicotinamide adenine dinucleotide phosphate (NADPH), also referred to as reduced coenzyme I and II, respectively.[2,29] They serve as crucial cofactors in numerous biochemical processes across living organisms, including plants and animals.[30] The pyridine ring, a key redox-active structure through the transfer of hydrogen anions (two electrons and one proton), plays a central role in their ability to store and transfer energy efficiently (Figure 1a).[31]

Nicotinic acid (NA) is the precursor of nicotinamide, the key redox-active unit of the coenzyme NAD(P)H. Its methylated derivative, NM, with a structure more closely resembling the redox-active moiety, has been therefore selected to assess its by electropositive nitrogen atoms in its pyridine ring, with its purity potential to undergo similar redox reactions (Figure 1b). Compared with NA molecules, the NM structure is distinguished confirmed by ^{1}H NMR spectrum (Figure S1a). The reduction of NM is monitored via ultraviolet-visible (UV–vis) absorption spectra, showcasing a distinct absorption peak at approximately 352 nm upon the addition of the strong reducing agent of $NaBH_4$.[32] This peak corresponds to the reduced form, NM[R], as verified by the theoretically simulated spectrum (Figure 1c). Furthermore, it is assumed that NM[R] has high reduction activity and is not easily stabilized; it is fortunately succeeded in attempting to capture its reduced state similar to dihydropyridine, via ^{1}H NMR spectrum in the presence of a reducing agent (Figure S1b).[33] The above observations demonstrate that NM exhibits redox-active characteristics analogous to NAD(P)$^+$ coenzymes, showing electron and proton transfer capabilities. This behavior suggests potential applications in designing artificial catalysts on appropriate supports, particularly in redox reaction systems requiring electron and proton transport mediation.

A representative MOF, UiO-66-NH_2, with the molecular formula $Zr_6O_4(OH)_4$(BDC-NH_2)$_6$, was first synthesized using a solvothermal method with $ZrCl_4$ and the linker 2-amino-1,4-benzenedicarboxylic acid (denoted as BDC-NH_2).[34,35] Following this, the NAD(P)H coenzyme analogues, NA and NM, were grafted onto the Zr-oxo clusters in UiO-66-NH_2 through carboxyl coordination by the solvent-assisted linker exchange (SALE) strategy,[36] affording UiO-66-X (X=NA, NM). The crystallinity of UiO-66-NH_2 is well inherited in resulting UiO-66-X based on powder X-ray diffraction (XRD), indicating that the framework remains stable after linker exchange (Figure S2). Scanning electron microscopy (SEM) observation reveals the similar octahedral morphology for all UiO-66-NH_2 and UiO-66-X (Figure S3). The incorporation of NA and NM in the MOF skeleton is verified by ^{1}H NMR results, where the molar ratio of -X to BDC-NH_2 linker is evaluated to be approximately 0.3:1 and 0.2:1, respectively (Figure S4). Additionally, the porous feature of UiO-66-NH_2 has been demonstrated by N_2 sorption, with a slight decrease in specific surface area after the SALE process (Figure S5).

There are negligible differences in light-harvesting efficiency among UiO-66-NH_2 and UiO-66-X, as demonstrated by the UV–vis absorption spectra (Figure S6a). Additionally, the desired incorporation of the NM has been confirmed

© 2025 Wiley-VCH GmbH

15213773, 2025, 40, Downloaded from https://onlinelibrary.wiley.com/doi/10.1002/anie.202511775 by University Of Science, Wiley Online Library on [07/10/2025]. See the Terms and Conditions (https://onlinelibrary.wiley.com/terms-and-conditions) on Wiley Online Library for rules of use; OA articles are governed by the applicable Creative Commons License

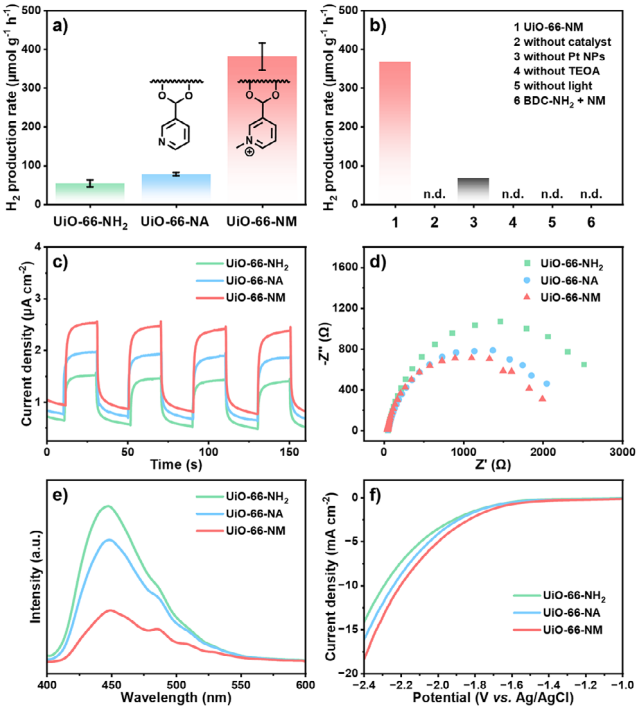

Figure 2. a) Photocatalytic H_2 production rates of UiO-66-NH_2 and UiO-66-X (X=NA, NM). The error bars represent the standard deviation of values obtained from three replicate experiments. Reaction conditions: 10 mg catalyst, 20 mL acetonitrile, 1 mL aqueous suspension solution of Pt NPs (0.05 mg mL^{-1}), 2 mL TEOA, 300 W xenon lamp ($\lambda \geq 380$ nm). b) Photocatalytic H_2 production activity of UiO-66-NM under the altered conditions ("n. d." represents "not detected"). c) Photocurrent responses, d) EIS Nyquist plots, e) steady-state photoluminescence emission spectra (under excitation at $\lambda = 380$ nm), f) LSV curves of UiO-66-NH_2 and UiO-66-X (X=NA, NM).

through Fourier transform infrared (FT-IR) spectra, as evidenced by characteristic peaks at 2964 and 1655 cm^{-1}, corresponding to the stretching and bending vibrations of the imine bond (—C=N—) in UiO-66-NM (Figure S7). Moreover, the successful grafting of the MOF with NAD(P)H mimics has been examined by zeta potential measurements; UiO-66-NM exhibits a slightly higher positive charge compared to the other two MOFs, attributed to the presence of the N^+ site in the NM structure (Table S1). Similarly, this is illustrated by the enhanced conductivity observed in UiO-66-NM (Table S2).

Motivated by the above results, photocatalytic hydrogen production by water splitting over UiO-66-NH_2 and UiO-66-X has been conducted in the presence of Pt NPs and triethanolamine (TEOA) under visible light irradiation to investigate the influence of the coenzyme mimics. The Pt nanoparticles (Pt NPs, ~4 nm) were pre-synthesized and used as a co-catalyst (Figure S8).

Strikingly, the three MOFs exhibit distinctly different activities in photocatalytic hydrogen production, in which UiO-66-NM gives the highest activity of 381 μmol g^{-1} h^{-1}, ~5.0 and 7.2 times higher than UiO-66-NA (77 μmol g^{-1} h^{-1}) and the pristine UiO-66-NH_2 (53 μmol g^{-1} h^{-1}), respectively, under the identical reaction conditions (Figure 2a). It is assumed that the N^+ species in the NM molecule behaving as coenzyme mimics is of the utmost importance for the activity enhancement. Control experiments demonstrate that all of the MOF catalyst (UiO-66-NM), co-catalyst (Pt NPs), sacrificial agent (TEOA), and light irradiation are essential for the photocatalytic hydrogen reaction (Figure 2b). It is worth mentioning that physically mixed samples of the photo-responsive linker BDC-NH_2 and NM also do not exhibit hydrogen production activity (reaction condition No. 6 in Figure 2b), supporting the hypothesis that the periodical structure of the MOF is crucial for the efficient separation of photogenerated carriers. Similarly, the necessity of the UiO-66-NM framework is supported by the lower catalytic activity observed in the physical mixture experiment of UiO-66-NH_2 and NM (Figure S9). UiO-66-NM displays recyclable performance in the photocatalytic hydrogen production (Figure S10). Meanwhile, the stability of UiO-66-NM has been demonstrated by powder XRD patterns, showing retained crystallinity even after five photocatalytic cycles (Figure S11). Moreover, there is no obvious leaching of linker (BDC-NH_2) or functional unit (NA or NM) during the photocatalysis have been confirmed by post-reaction liquid ^1H NMR, indicating the water stability of the material (Figure S12). The porosity of MOFs is also maintained after the reaction, as evidenced by the N_2 sorption isotherms (Figure S13). In addition, Pt NPs as a co-catalyst do not undergo obvious aggregation after the reaction, which is corroborated by TEM images (Figure S14).

To illuminate the charge transfer involved in UiO-66-NH_2 and UiO-66-X, their photoelectrochemical measurements have been conducted. Both UiO-66-NM and UiO-66-NA exhibit stronger photocurrent responses than the parent MOF with the order of UiO-66-NM > UiO-66-NA > UiO-66-NH_2 (Figure 2c), suggesting a higher efficiency of charge transfer in the former. This argument is also supported by the electrochemical impedance spectroscopy (EIS) measurements, where the radius of Nyquist plots follows a trend of UiO-66-NH_2 > UiO-66-NA > UiO-66-NM (Figure 2d), indicative of a lower charge-transfer resistance in the MOFs incorporating the coenzyme mimics. This is further supported by photoluminescence emission spectroscopy, which offers important information for photoexcited charge transfer and recombination. The steady-state photoluminescence emission spectra suggest reduced electron-hole recombination for UiO-66-NH_2 modified with coenzyme mimics (Figure 2e). The preceding outcomes indicate that the behaviors of electron-hole separation and charge transfer are consistent with the observed rates of photocatalytic water splitting for hydrogen production. In addition, the linear sweep voltammetry (LSV) measurement for electrochemical hydrogen production over UiO-66-NM exhibits the lowest overpotential, suggesting its superior proton reduction capability (Figure 2f). The above results jointly demonstrate that the introduction of coenzyme mimics, NA or NM, gives rise to enhanced charge separation efficiency, reduced charge transfer resistance, and improved proton reduction capability, which ultimately leads to the activity differences.

To elucidate the role of the NM coenzyme-regeneration-mimicking process in the photocatalytic reaction, time-resolved photoluminescence spectra measurements have been conducted (Figure 3a). The fitting results reveal the shortest lifetime of 1.30×10^{-10} s for UiO-66-NM, lower than

© 2025 Wiley-VCH GmbH

15213773, 2025, 40, Downloaded from https://onlinelibrary.wiley.com/doi/10.1002/anie.202511775 by University Of Science, Wiley Online Library on [07/10/2025]. See the Terms and Conditions (https://onlinelibrary.wiley.com/terms-and-conditions) on Wiley Online Library for rules of use; OA articles are governed by the applicable Creative Commons License

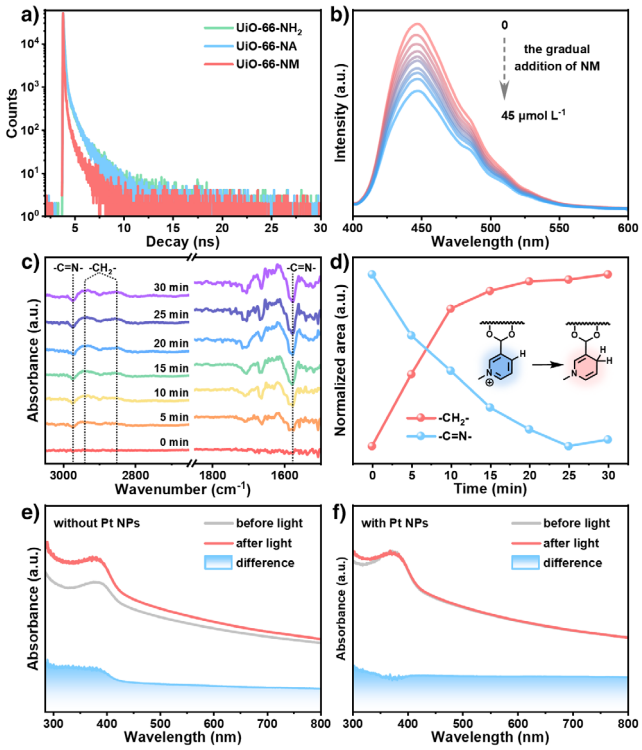

Figure 3. a) Time-resolved photo luminescence spectra (λ_{ex} = 373 nm, λ_{em} = 450 nm) of UiO-66-NH_2 and UiO-66-X (X=NA, NM). b) Fluorescence quenching experiment of UiO-66-NH_2 by introducing varying amounts of NM (0–45 μmol L^{-1}) upon excitation at 380 nm. c) In situ DRIFTS spectra for UiO-66-NM collected at different time lengths of visible light irradiation (0–30 min) and d) normalized peak area changes of the methylene —CH_2— and pyridine —C=N— characteristic peaks based on DRIFTS spectra. The stable infrared spectrum before light irradiation is recorded as background data for subtraction to clearly indicate spectral changes, and the inset shows the NM to NM[R] transition inferred from this. e), f) Quasi-in situ liquid-state UV–vis absorption and differential spectra for UiO-66-NM before and after visible light irritation under reaction conditions e) without Pt NPs and f) with Pt NPs.

that for UiO-66-NA and UiO-66-NH_2 (Table S3). This further suggests that electron transfer in UiO-66-NM occurs more rapidly than the other two counterparts, facilitating efficient separation of photogenerated carriers.[37] This conclusion is also supported by the open-circuit potential (OCP) decay curves upon light exposure, which demonstrate that UiO-66-NM has the shortest lifetime of photogenerated carriers (Figure S15). Given the above facts, upon adding varying amounts of NM molecules to a suspension of UiO-66-NH_2, significant reduction of the characteristic emission peak at around 450 nm is observed (Figure 3b), which indicates that photoexcited electrons might efficiently transfer from UiO-66-NH_2 to the NM molecules.

The band structures have been analyzed to disclose the photoinduced charge transfer pathways in UiO-66-X system. The band gap (E_g) can be evaluated from the Tauc plots (Figure S6b–d). Using the conduction band minimum (CBM) from Mott–Schottky plots, band structure can be assessed for the MOFs, confirming their thermodynamic suitability for photocatalytic hydrogen production (Figure S16). The reduction potential of NM has also been evaluated to be −0.39 V through cyclic voltammetry (CV) (Figure S17). This result suggests that photogenerated electrons originated from the MOF can migrate to reduce NM through thermodynamic path (Figure S18). To further investigate the intermediate changes between NM molecules and UiO-66-NH_2 during light irradiation, in situ diffuse reflectance infrared Fourier transform spectroscopy (DRIFTS) test has been conducted. For the pyridine —C=N— resonance peaks at 2974 and 1577 cm^{-1} in UiO-66-NM, after deducting the background spectrum, the gradually intensified negative peaks along with light irradiation actually indicate decreased absorbance signals (Figures 3c and S19), suggesting the disappearance of the —C=N— bond. Simultaneously, the emergence of two peaks centered at 2961–2820 cm^{-1} in the methylene (—CH_2—) stretching region is attributed to the hydrogenation of —CH=CH— bonds, resulting from the NM to NM[R] transition (Figure 3c). This provides direct evidence on the redox tautomeric structures of NM, similar to that of $NAD(P)^+$/NAD(P)H. The changes in the normalized peak area based on DRIFTS results visually reflect the transition of NM between the oxidized and reduced states (Figure 3d). In contrast, no similar trend can be observed for UiO-66-NH_2 and UiO-66-NA under identical conditions (Figure S20).

To prove that the coenzyme regeneration-like process occurs to UiO-66-NM, liquid-state UV–-vis absorption spectra have been also collected. By comparing the UiO-66-NM suspension solution with and without the reducing agent $NaBH_4$, the new characteristic peak can be observed at around 350 nm, which is assignable to the reduced state of NM (Figure S21). Quasi-in situ UV–vis absorption spectroscopy under light irradiation gives the new peak for NM[R] in the range of 300–400 nm through differential spectral analysis (Figure 3e). Upon adding the Pt co-catalyst, this signal decreases, which indicates that NM[R] is rapidly re-oxidized to NM, thereby suggesting that UiO-66-NM has self-healing capability (Figure 3f).

Based on the above findings, it is proposed that the photocatalytic process proceeds efficiently over UiO-66-NM involving the coenzyme mimics (Figure 4a). Under visible light irradiation, the photosensitive BDC-NH_2 linker is excited, causing proton and photogenerated electrons migration to NM, thereby forming NM[R]. Meanwhile, the holes are consumed by TEOA. Similar to coenzyme regeneration, the presence of Pt co-catalyst facilitates the redox cycle, allowing NM[R] to return to its oxidized state through proton and electron transfer while simultaneously driving hydrogen production, thereby completing the catalytic cycle. More intuitively, this photocatalytic process of UiO-66-NM can be demonstrated by the schematic chemical equations (Figure 4a, step 1–5), whereas UiO-66-NH_2, which lacks the coenzyme mimic, is correspondingly missing the key step involving the NM and NM[R] redox transitions.

Computational calculations are employed to understand the observed differences in catalytic activity among UiO-66-NH_2 and UiO-66-X. A time-dependent density functional theory (TD-DFT) calculation has been carried out to investigate the charge density distribution. The results of charge density distribution show that, while electrons and holes

© 2025 Wiley-VCH GmbH

15213773, 2025, 40, Downloaded from https://onlinelibrary.wiley.com/doi/10.1002/anie.202511775 by University Of Science, Wiley Online Library on [07/10/2025]. See the Terms and Conditions (https://onlinelibrary.wiley.com/terms-and-conditions) on Wiley Online Library for rules of use; OA articles are governed by the applicable Creative Commons License

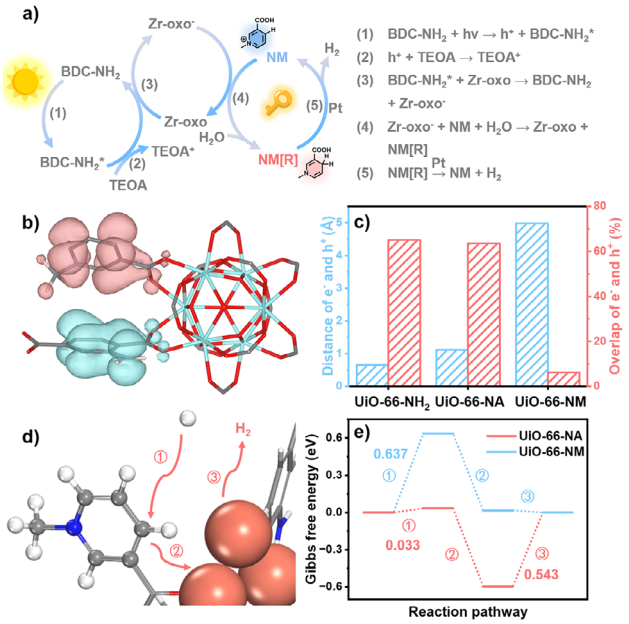

Figure 4. a) Proposed mechanism of photocatalytic hydrogen production over UiO-66-NM and corresponding chemical equations for each step on the right. b) Simulated electron-hole distribution diagrams of UiO-66-NM (cyan: Zr; gray: C; purple: N; red: O; light red area: electrons; light green area: holes, and H atoms are omitted for clarity. The iso surface value is 0.001 *e* $Bohr^{-3}$). c) The distance and overlapping percentage between electrons and holes in UiO-66-NH_2 and UiO-66-X (X=NA, NM). d) Simulated schematic diagram of hydrogen transfer over UiO-66-NM (orange: Pt; gray: C; blue: N; white: H). e) Calculated free energy diagram for hydrogen transfer over UiO-66-NA and UiO-66-NM.

on UiO-66-NH_2 and UiO-66-NA are closely coupled, the electron-hole pairs on UiO-66-NM are effectively separated (Figures 4b and S22), which are further confirmed by the distance and the overlapping percentage between electrons and holes (Figure 4c).[38] The enhanced charge separation suggests that photogenerated electrons on UiO-66-NM are readily migrated to NM, facilitating its reduction to NM[R] accompanied by rapid electron and proton transfer, which ultimately accelerates hydrogen production over the neighboring Pt clusters (Figures 4d and S23). These findings are supported by step-by-step calculations presented for the comparison (Figure 4e). UiO-66-NM, with high electron-hole separation level, readily interacts with protons, and its corresponding step 1 has a negligible Gibbs free energy change (ΔG = 0.033 eV). The rate- determining-step for the hydrogen production reaction over UiO-66-NM is step 3, which has the ΔG of 0.543 eV. In contrast, for UiO-66-NA, the rate-determining-step is the step 1, which requires a higher ΔG of 0.637 eV. Consequently, UiO-66-NM is more favorable for hydrogen production as demonstrated by ΔG comparison, aligning with its photocatalytic activity. These results highlight the crucial role of the dynamic coenzyme regeneration behavior between NM and NM[R] as the proton and electron relays,[39–41] which contributes significantly to the enhanced photocatalytic activity of UiO-66-NM.

To evaluate the significance and versatility of adopting the simulant of NAD(P)H cofactor, the NM molecules as

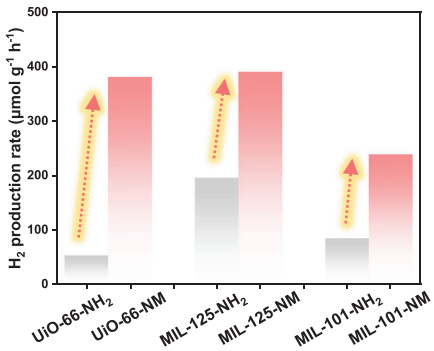

Figure 5. Photocatalytic H_2 production activity over diverse MOFs (UiO-66-NH_2, MIL-125-NH_2, and MIL-101-NH_2) with or without functionalization of NM molecules. Reaction conditions: 10 mg catalyst, 20 mL acetonitrile, 1 mL aqueous suspension solution of Pt NPs (0.05 mg mL^{-1}), 2 mL TEOA, and 300 W xenon lamp ($\lambda \geq 380$ nm).

coenzyme mimics have been grafted onto other MOF photocatalysts, such as MIL-125-NH_2 (based on Ti-oxo clusters) and MIL-101-NH_2 (with Al-oxo nodes). The crystallinity and morphology of these MOFs are well maintained during the post-synthetic modification based on powder XRD and SEM results (Figures S24 and S25). The successful incorporation of NM molecules into the MOFs has been verified by ^{1}H NMR spectra (Figure S26). Despite the differences in the photocatalytic MOF support, they lead to varying degrees of enhanced activity in photocatalytic hydrogen production after the rational introduction of NM by the SALE strategy (Figure 5). Specifically, MIL-125-NM exhibits 2.0 times increase in activity relative to MIL-125-NH_2, while MIL-101-NM also shows 2.8 times enhancement compared to MIL-101-NH_2. Although these improvements are less pronounced than that observed for UiO-66-NM relative to UiO-66-NH_2 (Table S4), they nevertheless underscore the broad applicability and effectiveness of the coenzyme-mimicking strategy.

Conclusion

In summary, the small molecules NA and NM, serving as the coenzyme NAD(P)H mimics, have been modified onto Zr-oxo clusters in UiO-66-NH_2 to afford UiO-66-NA and UiO-66-NM, respectively, for photocatalytic hydrogen production. Remarkably, the NM unit in UiO-66-NM enables efficient protons and electrons migration through photo-mediated redox reactions. As a result, UiO-66-NM exhibits a high hydrogen production rate up to 381 μmol g^{-1} h^{-1}, which is ~5.0 and ~7.2 times higher than that of UiO-66-NA and UiO-66-NH_2, respectively. Experimental and theoretical calculation results collectively demonstrate that the modification of coenzyme-mimicking NM onto the MOF photocatalyst promotes charge separation and the proton-coupled electron transfer (PCET) process, leading to improved hydrogen production. Importantly, drawing inspiration from these findings, the NM as coenzyme mimics can be modified onto diverse MOFs for improved photocatalytic hydrogen production, highlighting the excellent compatibility and versatility of this biomimetic catalysis strategy. From a biomimetic perspective,

© 2025 Wiley-VCH GmbH

15213773, 2025, 40, Downloaded from https://onlinelibrary.wiley.com/doi/10.1002/anie.202511775 by University Of Science, Wiley Online Library on [07/10/2025]. See the Terms and Conditions (https://onlinelibrary.wiley.com/terms-and-conditions) on Wiley Online Library for rules of use; OA articles are governed by the applicable Creative Commons License

this study departs from replicating complicated enzymatic structures, instead focusing on preserving their key functional units. The presented coenzyme regeneration strategy provides significant inspiration and guidance in the design and synthesis of advanced heterogeneous catalysts.

Acknowledgements

This work was supported by the Strategic Priority Research Program of the Chinese Academy of Sciences (XDB0540000 and XDB0450302), the National Key Research and Development Program of China (2021YFA1500402), the NSFC (22331009 and W2512006), the International Partnership Program of CAS (123GJHZ2022028MI), and the Postdoctoral Fellowship Program of CPSF (GZC20232532). The authors gratefully acknowledge the Supercomputing Center at the University of Science and Technology of China (USTC) and the Hefei Advanced Computing Center for providing computational resources. Portions of this work were conducted at the Instruments Center for Physical Science of USTC.

Conflict of Interests

The authors declare no conflict of interest.

Data Availability Statement

The data that support the findings of this study are available from the corresponding author upon reasonable request.

Keywords: Hydrogen production · Metal-organic frameworks · Microporous materials · Photocatalysis · Proton and electron relays

[1] R. B. Leveson-Gower, C. Mayer, G. Roelfes, *Nat. Rev. Chem.* **2019**, *3*, 687–705.
[2] M. A. Emmanuel, N. R. Greenberg, D. G. Oblinsky, T. K. Hyster, *Nature* **2016**, *540*, 414–417.
[3] R. J. Drout, L. Robison, O. K. Farha, *Coord. Chem. Rev.* **2019**, *381*, 151–160.
[4] E. L. Bell, W. Finnigan, S. P. France, A. P. Green, M. A. Hayes, L. J. Hepworth, S. L. Lovelock, H. Niikura, S. Osuna, E. Romero, K. S. Ryan, N. J. Turner, S. L. Flitsch, *Nat. Rev. Methods Primers* **2021**, *1*, 46.
[5] Q. Zhu, P. Dong, J. Yu, Z. Wang, T. Wang, S. Qiao, J. Liu, S. Geng, Y. Zheng, P. Cheng, M. J. Zaworotko, Z. Zhang, Y. Chen, *Nat. Commun.* **2025**, *16*, 992.
[6] R. Breslow, L. E. Overman, *J. Am. Chem. Soc.* **1970**, *92*, 1075–1077.
[7] R. Breslow, *Chem. Soc. Rev.* **1972**, *1*, 553.
[8] V. Köhler, Y. M. Wilson, M. Dürrenberger, D. Ghislieri, E. Churakova, T. Quinto, L. Knörr, D. Häussinger, F. Hollmann, N. J. Turner, T. R. Ward, *Nat. Chem.* **2013**, *5*, 93–99.
[9] K. Chen, F. H. Arnold, *Nat. Catal.* **2020**, *3*, 203–213.
[10] T. Knaus, C. E. Paul, C. W. Levy, S. De Vries, F. G. Mutti, F. Hollmann, N. S. Scrutton, *J. Am. Chem. Soc.* **2016**, *138*, 1033–1039.
[11] Y. Zhang, Y. Jiang, A. Nafady, Z. Tang, A. M. Al-Enizi, K. Tan, S. Ma, *ACS Cent. Sci.* **2023**, *9*, 1692–1701.
[12] L. Zhao, J. Cai, Y. Li, J. Wei, C. Duan, *Nat. Commun.* **2020**, *11*, 2903.
[13] A. Rodriguez-Abetxuko, A. Reifs, D. Sánchez-deAlcázar, A. Beloqui, *Angew. Chem. Int. Ed.* **2022**, *61*, e202206926.
[14] J. Wei, L. Zhao, Y. Zhang, G. Han, C. He, C. Wang, C. Duan, *J. Am. Chem. Soc.* **2023**, *145*, 6719–6729.
[15] J. Sheng, Y. Wu, H. Ding, K. Feng, Y. Shen, Y. Zhang, N. Gu, *Adv. Mater.* **2024**, *36*, 2211210.
[16] W. Wang, R. Tachibana, K. Zhang, K. Lau, F. Pojer, T. R. Ward, X. Hu, *Angew. Chem. Int. Ed.* **2025**, *64*, e202422783.
[17] Y. Huang, J. Ren, X. Qu, *Chem. Rev.* **2019**, *119*, 4357–4412.
[18] J. Wu, X. Wang, Q. Wang, Z. Lou, S. Li, Y. Zhu, L. Qin, H. Wei, *Chem. Soc. Rev.* **2019**, *48*, 1004–1076.
[19] T. Vornholt, F. Leiss-Maier, W. J. Jeong, C. Zeymer, W. J. Song, G. Roelfes, T. R. Ward, *Nat. Rev. Methods Primers* **2024**, *4*, 78.
[20] H.-C. Zhou, J. R. Long, O. M. Yaghi, *Chem. Rev.* **2012**, *112*, 673–674.
[21] H. Furukawa, K. E. Cordova, M. O'Keeffe, O. M. Yaghi, *Science* **2013**, *341*, 1230444.
[22] I. Nath, J. Chakraborty, F. Verpoort, *Chem. Soc. Rev.* **2016**, *45*, 4127–4170.
[23] K. Chen, C.-D. Wu, *Coord. Chem. Rev.* **2019**, *378*, 445–465.
[24] G. Lan, Y. Fan, W. Shi, E. You, S. S. Veroneau, W. Lin, *Nat. Catal.* **2022**, *5*, 1006–1018.
[25] L. Jiao, J. Wang, H.-L. Jiang, *Acc. Mater. Res.* **2021**, *2*, 327–339.
[26] S. Hu, J. Huang, M.-L. Gao, Z. Lin, Y. Qian, W. Yang, L. Jiao, H.-L. Jiang, *Angew. Chem. Int. Ed.* **2025**, *64*, e202415155.
[27] X. Zhao, R. Gao, H. Sun, P. Chen, H. Zheng, L. Meng, *Coord. Chem. Rev.* **2025**, *533*, 216539.
[28] K.-Y. Wang, J. Zhang, Y.-C. Hsu, H. Lin, Z. Han, J. Pang, Z. Yang, R.-R. Liang, W. Shi, H.-C. Zhou, *Chem. Rev.* **2023**, *123*, 5347–5420.
[29] X. Cao, L. Wu, J. Zhang, M. Dolg, *J. Comput. Chem.* **2020**, *41*, 305–316.
[30] Y. Maenaka, T. Suenobu, S. Fukuzumi, *J. Am. Chem. Soc.* **2012**, *134*, 367–374.
[31] C. E. Paul, I. W. C. E. Arends, F. Hollmann, *ACS Catal.* **2014**, *4*, 788–797.
[32] J. Liu, C. Guo, X. Hu, G. Zhao, *Green Chem.* **2019**, *21*, 339–348.
[33] C. E. Paul, S. Gargiulo, D. J. Opperman, I. Lavandera, V. Gotor-Fernández, V. Gotor, A. Taglieber, I. W. C. E. Arends, F. Hollmann, *Org. Lett.* **2013**, *15*, 180–183.
[34] J. H. Cavka, S. Jakobsen, U. Olsbye, N. Guillou, C. Lamberti, S. Bordiga, K. P. Lillerud, *J. Am. Chem. Soc.* **2008**, *130*, 13850–13851.
[35] T. He, X. Xu, B. Ni, H. Wang, Y. Long, W. Hu, X. Wang, *Nanoscale* **2017**, *9*, 19209–19215.
[36] S. Takaishi, E. J. DeMarco, M. J. Pellin, O. K. Farha, J. T. Hupp, *Chem. Sci.* **2013**, *4*, 1509.
[37] M. Xu, D. Li, K. Sun, L. Jiao, C. Xie, C. Ding, H.-L. Jiang, *Angew. Chem. Int. Ed.* **2021**, *60*, 16372–16376.
[38] Y. Pan, J. Wang, S. Chen, W. Yang, C. Ding, A. Waseem, H.-L. Jiang, *Chem. Sci.* **2022**, *13*, 6696–6703.
[39] X.-M. Li, L.-Z. Dong, J. Liu, W.-X. Ji, S.-L. Li, Y.-Q. Lan, *Chem* **2020**, *6*, 2272–2282.
[40] H.-L. Zhu, H.-Y. Chen, Y.-X. Han, Z.-H. Zhao, P.-Q. Liao, X.-M. Chen, *J. Am. Chem. Soc.* **2022**, *144*, 13319–13326.
[41] J. Y. Choi, M. Stodolka, N. Kim, H. T. B. Pham, B. Check, J. Park, *Chem* **2023**, *9*, 143–153.

Manuscript received: May 29, 2025
Revised manuscript received: July 20, 2025
Accepted manuscript online: August 05, 2025
Version of record online: August 18, 2025

© 2025 Wiley-VCH GmbH

15213773, 2025, 40, Downloaded from https://onlinelibrary.wiley.com/doi/10.1002/anie.202511775 by University Of Science, Wiley Online Library on [07/10/2025]. See the Terms and Conditions (https://onlinelibrary.wiley.com/terms-and-conditions) on Wiley Online Library for rules of use; OA articles are governed by the applicable Creative Commons License